Available Online

J. Sci. Res. **14** (3), 797-812 (2022)

JOURNAL OF SCIENTIFIC RESEARCH

www.banglajol.info/index.php/JSR

Effects on Unsteady MHD Flow of a Nanofluid for Free Convection past an Inclined Plate

S. M. O. Gani[1,2*], M. Y. Ali[2], M. A. Islam[1,2]

[1]Department of Natural Science, Port City International University, Chittagong, Bangladesh

[2]Department of Mathematics, Chittagong University of Engineering & Technology, Chittagong-4349, Bangladesh

Received 17 February 2022, accepted in final revised form 17 June 2022

Abstract

This paper deals with a similarity solution of unsteady magneto hydrodynamics two-dimensional boundary layer flow of a nanofluid for free convection past an inclined plate. Using similarity transformations, the governing equations are reduced into a set of non-linear ordinary differential equations. The transformed dimensionless equations are then solved numerically using the Nachtsheim-Swigert iteration technique and the order Runga-Kutta method. The effects of buoyancy-ratio parameter, Magnetic parameter, Brownian motion parameter, Thermophoresis parameter, Brownian diffusion parameter, unsteadiness, and other driving parameters on the velocity profile, temperature profile, and concentration profile are represented graphically and discussed in detail. The numerical values of several involved parameters on Skin-friction co-efficient, local Nusselt, and Sherwood numbers are presented in tabular form.

Keywords: Unsteady; Magneto hydrodynamics; Inclined plate; Nanofluid; Convection; Boundary layer flow.

doi: http://dx.doi.org/10.3329/jsr.v14i3.58301 J. Sci. Res. **14** (3), 797-812 (2022)

1. Introduction

We have examined the influence of nanoparticles on natural convection boundary-layer flow past a vertical plate. Nanofluids are thought to have a wide range of advantages in medical applications, biomedical industry, detergency, power generation in nuclear reactors, and more specifically, in any heat removal involved in industrial applications. The ongoing research will focus on the utilization of nanofluids in microelectronics, fuel cells, pharmaceutical processes, hybrid-powered engines, engine cooling, vehicle thermal management, domestic refrigerator, chillers, heat exchanger, nuclear reactor coolant, grinding, machining, space technology, defense and ships, and boiler flue gas temperature reduction [1]. Choi *et al.* [2] first introduced the concept of nanofluids where he proposed the suspension of nanoparticles in a base fluid such as water, oil, and ethylene glycol. Kuznetsov *et al.* [3] have examined the influence of nanoparticles on natural convection

* *Corresponding author*: ganiosman3175@gmail.com

boundary-layer flow past a vertical plate. Uddin *et al.* [4] discussed Steady two-dimensional MHD laminar free convective boundary layer flows of an electrically conducting Newtonian nanofluid over a solid stationary vertical plate. Mustafa *et al.* [5] studied Non-linear radiation heat transfer effects in the natural convective boundary layer flow of nanofluid past a vertical plate: a numerical study. Rana *et el.* [6] studied a numerical study of a nanofluid's flow and heat transfer over a nonlinearly stretching sheet. Shit *et al.* [7] have analyzed the viscoelastic nanofluid flow and heat transfer over a stretching sheet in a magnetic field. Goyal *et al*. [8] considered a numerical solution of MHD viscoelastic nanofluid flow over a stretching sheet with partial slip and heat source/sink.

Wang *et al*. [9] analyzed the effect of electric fields and magnetic fields on the heat transfer of nanofluids, the mechanism of thermal conductivity enhancement of nanofluids, and the heat transfer enhancement of nanofluids in the presence of an applied electric field. Nandy *et al*. [10] studied unsteady forced convection nanofluid's two-dimensional boundary layer flow over a permeable, shrinking sheet of thermal radiation. Ibrahim *et al.* [11] studied similar heat and mass transfer solutions for natural convection over a moving vertical plate with internal heat generation and a convective boundary condition in the presence of thermal radiation, viscous dissipation, and chemical reaction. Boundary layer flow and heat transfer of viscoelastic nanofluids past a stretching sheet with partial slip conditions were discussed by Goyal *et al*. [12]. Goyal *et al*. [13] analyzed the boundary layer flow of nanofluids over a power-law stretching sheet effect on coating and suspensions, movement of biological fluid, cooling of the metallic plate, melt-spinning, heat exchangers technology, and oceanography. Ali *et al*. [14] have considered the combined effects of radiation and chemical reaction on the magnetohydrodynamic free convection flow of an electrically conducting incompressible viscous fluid over an inclined plate embedded in a porous medium.

Thermophoresis is a radiometric force by a temperature gradient that enhances small micron-sized particles moving toward a cold surface and away from the hot surface. The deposition efficiency of small particles due to thermophoresis in a laminar tube flow was calculated by Walker *et al*. [15]. Hamad *et al.* [16] obtained Magnetic field effects on the free convection flow of a nanofluid past a vertical semi-infinite flat plate. Steady natural convection boundary-layer flow of a nanofluid consisting of a pure fluid with nanoparticles along with a permeable verticle plate in the presence of the magnetic field, heat generation or absorption, and suction or injection effects have been analyzed by Chamkha *et al*. [17]. Ali *et al*. [18] Hence, analyzing unsteady two dimensions free convective boundary layer flow along with a permeable inclined flat plate in magnetic field and thermophoresis is greatly important. Stability analysis and its direct simulation were analyzed by Venkatasubbaiah *et al*. [19]. Johnson *et al*. [20] investigated possible similarity solutions for free convection boundary layers adjacent to flat plates in porous media. Kumari *et al.* [21] have studied unsteady free convection flow over a continuous moving vertical surface. Slaouti *et al*. [22] considered unsteady free convection flow in the stagnation-point region of a three-dimensional body. Hamad *et al*. [23] examined

unsteady MHD free convection flow past a vertical permeable flat plate in a rotating frame of reference with a constant heat source in a nanofluid.

Very Recently, Ali *et al*. [24-26] studied similarity solutions for internal heat generation, thermal radiation, and free convection unsteady boundary layer flow over a vertical plate. Further, we also examined similarity solutions of unsteady convective boundary layer flow along with the isothermal vertical plate with porous medium. Moreover, we considered similarity solutions of unsteady mixed convective boundary layer flow of viscous incompressible fluid along with an isothermal horizontal plate.

The present study aims to discuss the effect of a similarity solution of unsteady MHD boundary layer flow of a nanofluid for free convection around an inclined plate. In this study, the governing partial differential equations are transformed into a system of non-linear ordinary differential equations by using similarity transformation. The transformed equations are solved by using the Shooting Technique. The results of non-dimensional parameters on the velocity, temperature, and concentration profiles, magnetic parameter, Prandtl number, Brownian motion parameter, buoyancy-ratio parameter, thermophoresis parameter, Brownian diffusion parameter, unsteadiness and other driving parameters, Skin-friction co-efficient, Nusselt and Sherwood numbers are observed and presented with graphs.

2. Mathematical Problem, Governing Equations, and Boundary Conditions

In this paper, we discussed unsteady, incompressible, two-dimensional, and laminar with constant physical properties. The semi-infinite plate is inclined at an acute angle d to the vertical axis. With the x-axis measured along with the plate, a magnetic field of uniform strength B_0 is applied in the y-direction (normal to the flow direction). The gravitational acceleration g_e is acting downward. In addition, the buoyancy effects are included in momentum transfer with the usual Boussinesq approximation. It is assumed that the plate's lower side is heated by convection through a hot fluid at the temperature T_f and with a coefficient of heat transfer h_f. The nanoparticles and base fluid are assumed to be in thermal equilibrium. In the vicinity of the plate, three different types of boundary layers (momentum, thermal, and nanoparticle volume (fraction) are formed.

Upon incorporating the main assumptions into the conversation equations for mass, momentum, thermal energy, and nanoparticle species, the dimensional set of governing equations is written as:

$$\frac{\partial u}{\partial x}+\frac{\partial v}{\partial y}=0 \tag{1}$$

$$\frac{\partial u}{\partial t}+\rho_f\left(u\frac{\partial u}{\partial x}+v\frac{\partial u}{\partial y}\right)=\mu\frac{\partial^2 u}{\partial y^2}-\sigma_{nf}B_0^2u+[\left(1-\widehat{\emptyset}_\infty\right)\rho_{f_\infty}\beta g_e(T-T_\infty)-$$
$$(\rho_p-\rho_{f_\infty})g_e(\widehat{\emptyset}-\widehat{\emptyset}_\infty)]cosd. \tag{2}$$

$$\frac{\partial T}{\partial t}+u\frac{\partial T}{\partial x}+v\frac{\partial T}{\partial y}=\alpha_m\frac{\partial^2 T}{\partial y^2}+\tau[Db\frac{\partial\widehat{\emptyset}}{\partial y}\frac{\partial T}{\partial y}+\frac{D_T}{T_\infty}\left(\frac{\partial T}{\partial y}\right)^2] \tag{3}$$

$$\frac{\partial \widehat{\emptyset}}{\partial t} + u\frac{\partial \widehat{\emptyset}}{\partial x} + v\frac{\partial \widehat{\emptyset}}{\partial y} = Db\frac{\partial^2 \widehat{\emptyset}}{\partial y^2} + \frac{D_T}{T_\infty}\frac{\partial^2 T}{\partial y^2} \quad (4)$$

Where u and v are the velocity components parallel and perpendicular to the plate, respectively, B_0 is uniform magnetic field strength, $\widehat{\emptyset}$ is the local solid volume fraction of the nanoparticles, β is the volumetric thermal expansion coefficient of the base fluid, Db is the Brownian diffusion Coefficient, D_T is the thermophoretic diffusion coefficient, and T is the local temperature. Db Brownian diffusion coefficient. Continuity, momentum, thermal energy, and nanoparticle species equations for nanofluids are represented by equations. (1)-(4).

The boundary conditions may be written as

$$u = 0, v = 0, \widehat{\emptyset} = \widehat{\emptyset}_w, T = T_f \; at \; y = 0. \quad (5)$$

$$u = 0, v = 0, \widehat{\emptyset} = \widehat{\emptyset}_\infty, T = T_\infty at \; y \to \infty. \quad (6)$$

The continuity equation (1) is satisfied by introducing the steam function$\Psi(x, y)$. Such that

$$u = \frac{\partial \Psi}{\partial y}, v = -\frac{\partial \Psi}{\partial x}. \quad (7)$$

The momentum, thermal energy, and nanoparticles species equations can be transformed to the corresponding ordinary differential equations by introducing the following Similarity transformations:

$$\eta = \frac{y}{xt}(R_{a_x})^{1/4}, \; \psi = \alpha_m\left(R_{a_x}\right)^{1/4} f(\eta), \; \theta(\eta) = \frac{T - T_\infty}{T_f - T_\infty}, \; \emptyset(\eta) = \frac{\widehat{\emptyset} - \emptyset_\infty}{\widehat{\emptyset}_w - \widehat{\emptyset}_\infty}. \quad (8)$$

With the local Rayleigh number is defined as

$$R_{a_x} = \frac{(1-\widehat{\emptyset}_\infty)\beta g_e (T_f - T_\infty) x^3 t^3}{\nu \alpha_m} \quad (9$$

The momentum, thermal energy, and nanoparticles species equations (2)-(4), after some simplifications reduce to the following forms:

$$f''' + (\theta - Nr\emptyset)cosd - Mf' + \frac{1}{E}[P]^{-1/2}(f' + \eta f'') + \frac{1}{Pr}f'^2 = 0 \quad (10)$$

$$\theta'' + Nb\theta'\emptyset' + Nt\theta'^2 + \frac{1}{Bm}[P]^{-1/2}\eta\theta' = 0 \quad (11)$$

$$\emptyset'' + \frac{Nt}{Nb}\theta'' + \frac{1}{Db}[P]^{-1/2}\eta\emptyset' = 0 \quad (12)$$

$$\text{Where, } Pr(\text{Modified Prandtl Number}) = \frac{\mu}{\alpha_m \rho_f t} \quad (13)$$

$$M(\text{Modified Magnetic field Parameter}) = \frac{\sigma_{nf} B_0^2 x^2 t^2}{\mu (R_{a_x})^{\frac{1}{2}}} \quad (14)$$

$$Nr(\text{Buoyancy} - \text{ratio parameter}) = \frac{(\rho_p - \rho_f)(\widehat{\emptyset}_w - \widehat{\emptyset}_\infty)}{\rho_{f_\infty}(1-\widehat{\emptyset}_\infty)(T_f - T_\infty)} \quad (15)$$

$$Nb(\text{Brownian motion parameter}) = \frac{\tau D_B(\widehat{\emptyset}_w - \widehat{\emptyset}_\infty)}{\alpha_m} \quad (16)$$

$$Nt(\text{thermophoresis parameter}) = \frac{\tau D_T (T_f - T_\infty)}{T_\infty \alpha_m} \quad (17)$$

$$\text{Bm}(\text{thermal diffusivity parameter}) = \frac{t}{x} \quad (18)$$

$$E(\text{Viscosity of the nanofluid}) = \mu \quad (19)$$

$$\text{And unsteadiness parameter} P = \frac{(1-\widehat{\emptyset}_\infty)\beta g_e (T - T_\infty)}{\mu} \quad (20)$$

The corresponding boundary conditions are:

$$f(\eta) = 0,\ f'(\eta) = 0,\ \theta(\eta) = 1,\ \theta'(\eta) = 0,\ \emptyset(\eta) = 1,\ at\ \eta = 0 \quad (21)$$

$$f'(\eta) = 0,\ \theta(\eta) = 0,\ \emptyset(\eta) = 0\ as\ \eta \to \infty \quad (22)$$

Where the prime (') denotes differentiation with respect to η.

The above equations with boundary conditions are solved numerically by using the shooting technique.

3. Skin-Friction Coefficient, Nusselt, and Sherwood Number Evaluation

The quantities we are interested in studying are the Skin-friction co-efficientC_f, local Nusselt number Nu_x and the local Sherwood number $Sh_{x,n}$. These parameters respectively characterize wall heat and mass transfer rates. The quantities are defined as:

$$C_f = \frac{\tau_w}{\rho u^2},\ Nu_x = \frac{x q_w}{k(T_f - T_\infty)},\ Sh_{x,n} = \frac{x q_{np}}{D_B(\widehat{\emptyset_w} - \widehat{\emptyset_\infty})} \quad (23)$$

Where τ_w, q_m and q_{np} are the local shearing stress, wall heat, and nano mass fluxes, respectively.

The modified Skin-friction co-efficient C_f, Nusselt number Nur and modified nanoparticle Sherwood number $Shrn$ can be written as:

$$C_f {Ra_x}^{1/4} = f''(0),\ Nur = {Ra_x}^{1/4} Nu_x = -\theta'(0), Shrn = {Ra_x}^{1/4} Sh_{x,n} = -\emptyset'(0) \quad (24)$$

4. Numerical Solution

The systems of non-linear ordinary differential equations together with boundary conditions are coupled. Firstly, higher-order non-linear differential equations are converted into linear differential equations of the first order. These are further transformed into initial value problems solved numerically by applying the shooting method, namely Nachtsheim-Swigert (1965) iteration technique (guessing the missing value) along with the sixth-order Runga-Kutta integration technique. Nachtsheim-Swigert iteration technique is used as the main tool for the numerical approach. The dimensionless similarity equations for momentum, temperature, and concentration are solved numerically using the iteration technique.

In the shooting technique, the missing initial condition at the initial point of the interval is assumed. The differential equations are also integrated numerically as an initial value problem to the terminal point. The accuracy of the assumed missing initial condition is then checked by comparing the calculated value of the dependent variable at the

terminal point with its given value. If a difference exists, another value of the missing initial condition must be assumed; thus, the process is repeated. This process is continued until an agreement between the calculated and the given condition for the specified degree of accuracy. The corresponding velocity, temperature, and concentration profiles are shown in the figures.

5. Results and Discussion

In this paper, we studied the unsteady MHD boundary layer flow of a nanofluid for free convection past an inclined plate. The transformed sets of non-linear ordinary differential equations with boundary conditions are solved numerically using the shooting method. The velocity, temperature, concentration profiles, skin-friction coefficient, Nusselt number, and Sherwood number were discussed for different flow parameters involved in the problem. The effects of various parameters are shown graphically and in tabular form.

The effect of the different parameters are shown graphically in Fig. 1 to Fig. 27 by considering M=0.10, Pr=5.0, Nr=0.50, E=0.01, Nb=0.50, P=0.60, Nt=0.50, Bm=0.10, Db=0.10, d=60.0.

Fig. 1 illustrates the velocity profile for different values of the Brownian diffusion coefficient *Db*. The key property of Brownian diffusion is the thermal motion of droplets. The increasing Brownian diffusion coefficient *Db* causes an increasing velocity profile. Fig. 2 represents the dimensionless temperature profile for several values of the Brownian diffusion coefficient *Db*, the temperature profile decrease with increases in *Db*. Fig. 3 displays the effects of Brownian diffusion coefficient *Db* on the concentration profile. This is represented in the increase of the concentration profile as the Brownian diffusion coefficient Db increases.

In Fig. 4, the effect of the velocity profile for different values of the thermal diffusivity parameter Bm. Thermal diffusivity is the thermal conductivity separated by density and specific heat capacity at constant pressure. The thermal diffusivity slightly increased with increasing temperature. The velocity profile decreases with Bm increases. Fig. 5 reveals the effect of the thermal diffusivity parameter Bm on the temperature profile. It is evident from the figure that an increase in the thermal diffusivity parameter Bm improves the temperature profile. Fig. 6 shows the effect of thermal diffusivity parameter Bm on concentration profile. As *Bm* increases, the concentration profile decreases but at a certain time, the concentration profile reverse.

The Thermophoresis parameter is the conveyance force that arises due to a temperature gradient. Fig. 7 illustrates the influence of the thermophoresis parameter *Nt* on the velocity profile of the flow. It is clear from the figure that an increase in the thermophoresis parameter *Nt* raises the velocity profile of the flow. Fig. 8 shows the influence of the thermophoresis parameter *N*t on the temperature profile of the flow. The temperature profile enhances with an increase of the thermophoresis parameter *Nt*. The influence of the thermophoresis parameter, *Nt* on the concentration profile is plotted in Fig. 9. As the thermophoresis parameter Nt increases concentration profile increases.

Fig. 10 illustrates the velocity profile for different values of the unsteadiness parameter *P*. This figure reveals that an increase in unsteadiness parameter *P* results in a decrease in velocity profile. Fig. 11 shows the effect of the unsteadiness parameter *P* on the temperature profile and increases the unsteadiness parameter, but there is no significant variation in the temperature profile. Fig. 12 represents the variation of the concentration profile with the unsteadiness parameter. It noted that as *P* increases, the concentration profile decreases.

Brownian motion is the random motion of nanoparticles inside the base fluid due to the nonstop crash of nanoparticles with the molecules of the base fluid. This motion of the particles is defined by parameter Nb, Also known as the Brownian motion coefficient. Fig. 13 elucidate the velocity profile for the several values of the Brownian motion parameter Nb. It is clearly shown in the figure that the Brownian motion parameter increases, and the velocity profile increases. Fig. 14 illustrates the effect of the Brownian motion parameter on the temperature profile. As shown in the figure, the temperature profile increases with increasing values of the Brownian motion parameter. The effect of the Brownian motion parameter Nb on the concentration profile is shown in Fig. 15. An increase in the Brownian motion parameter decreases the concentration profile, but at a certain time, the concentration profile is reversed.

The viscosity of the nanofluid is created on the hypothesis of viscous fluid containing spherical particles at a very low volume fraction. Fig. 16 displays the variation of velocity profiles for different viscosity values of the nanofluid *E*. We observe that the velocity profiles increase swiftly with the increase of the viscosity of the nanofluid. The effect of the viscosity of the nanofluid (*E*) on temperature profiles have shown in Fig. 17. It is clear that there is an enhancement in the viscosity of the nanofluid, but there is no variation in the temperature profiles. Fig. 18 reveals the effect of the viscosity of the nanofluid (*E*) on the concentration profiles. It is evident from the figure that there is an increase in the viscosity of the nanofluid, but it does not show any effect on the concentration profiles.

The ratio of the variation of the fluid density to the variation of the nanofluid is defined by the buoyancy-ration parameter *Nr*. Fig. 19 shows the effect of the Buoyancy-ratio parameter *Nr* on velocity profiles. As shown in the figure, velocity profiles increase with increasing values of Buoyancy-ratio parameter Nr. The influence of the Buoyancy-ratio parameter *Nr* on the temperature profiles is plotted in Fig. 20. With the increasing Buoyancy-ratio parameters, temperature profiles show no significant variation. Fig. 21 represents typical concentration profiles for various values of the Buoyancy-ratio parameter *Nr*. We see that the concentration profiles increase with the Buoyancy-ratio parameter Nr, but the increment is very small.

Lorentz force is a resistive force created due to magnetic field decreases the fluid motion in the boundary layer region. Fig. 22 depicts the effect of the magnetic field parameter (*M*) on the velocity profiles. It is observed that the velocity profile is reduced with increasing values of the magnetic field parameter (*M*). Fig. 23 exhibits the temperature profiles' magnetic field parameter (*M*). The temperature profile is accelerated with the increase of the magnetic field parameter (*M*), and the increment is very small.

Fig. 24 displays the effect of the magnetic field parameter (M) on concentration profiles. As the magnetic field parameter (M) increases, there is no variation in the concentration profiles.

The influence of angle (d) on the velocity profile is shown in Fig. 25. It is observed that the velocity profile of the fluid decreases with increasing angle (d). As the angle of inclination rises, the influence of the buoyancy force due to thermal diffusion decreases. Figs. 26 and 27 show the effect of the temperature and concentration profiles. Obviously, there is no variation in the temperature and concentration profiles in the presence of an angle.

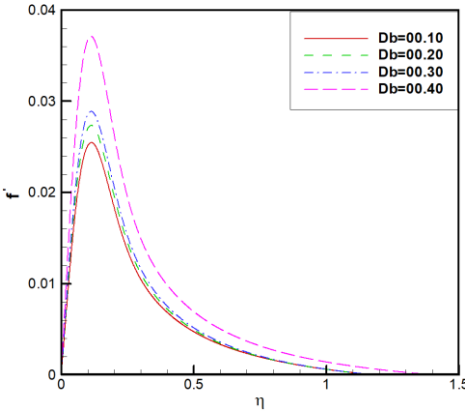

Fig. 1. Velocity profile for different values of Db.

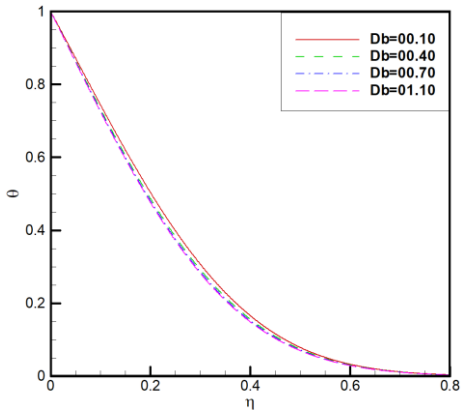

Fig. 2. Temperature profile for different values of Db.

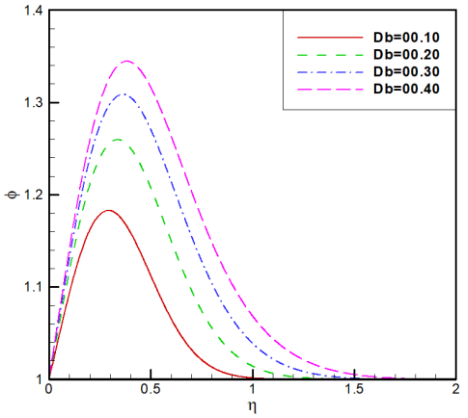

Fig. 3. Concentration profile for different values of Db.

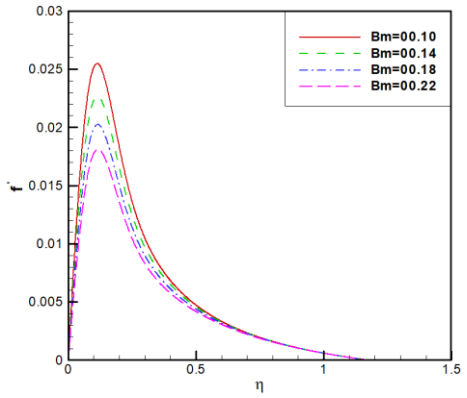

Fig. 4. Velocity profile for different values of Bm.

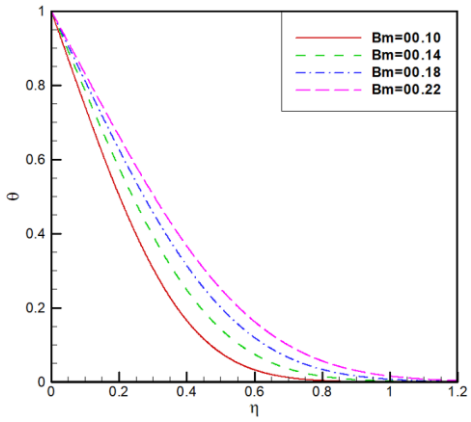

Fig. 5. Temperature profile for different values of Bm.

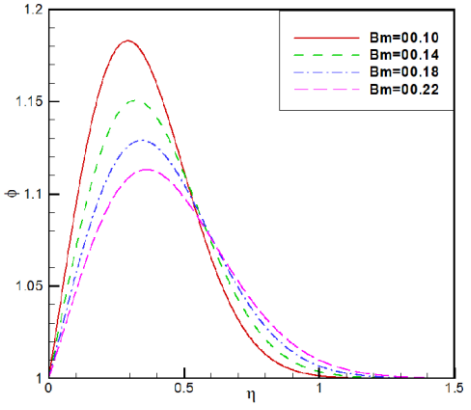

Fig. 6. Concentration profile for different values of Bm.

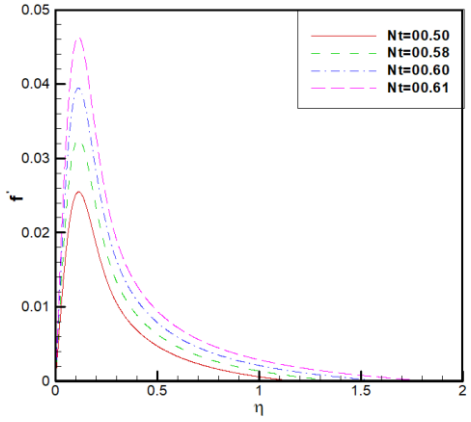

Fig. 7. Velocity profile for different values of Nt.

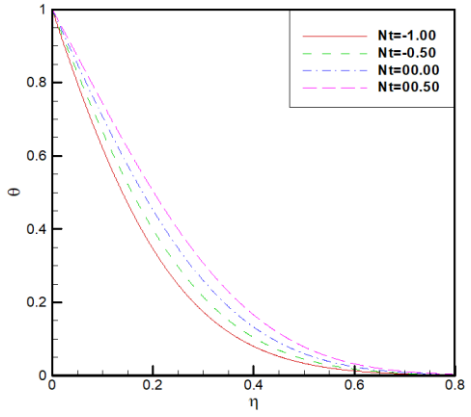

Fig. 8. Temperature profile for different values of Nt.

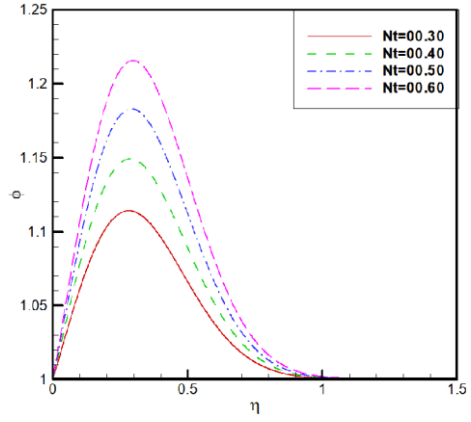

Fig. 9. Concentration profile for different values of Nt.

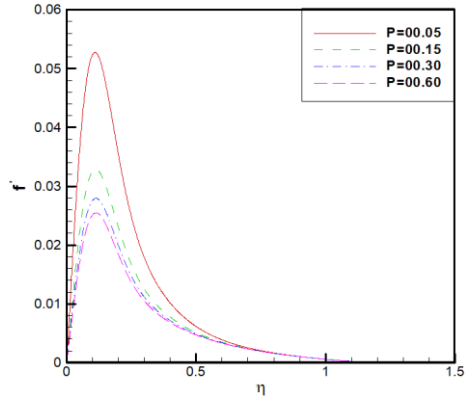

Fig. 10. Velocity profile for different values of P.

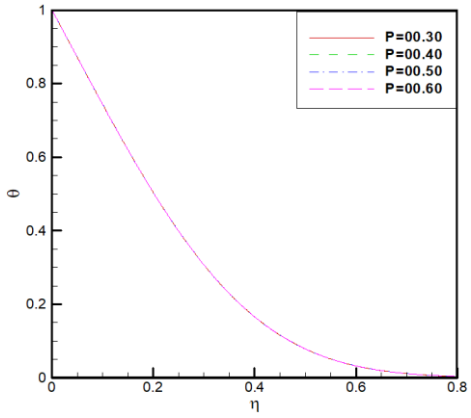

Fig. 11. Temperature profile for different values of P.

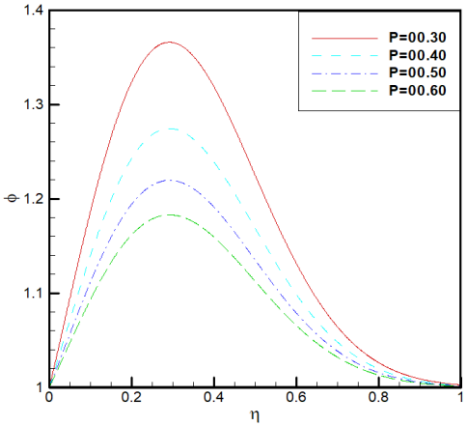

Fig. 12. Concentration profile for different values of P.

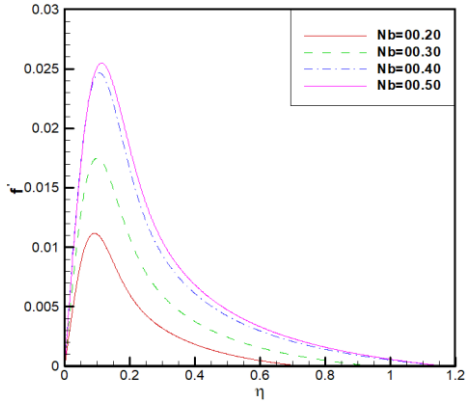

Fig. 13. Velocity profile for different values of Nb.

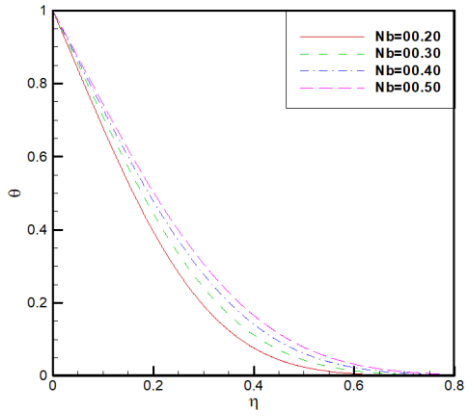

Fig. 14. Temperature profile for different values of Nb.

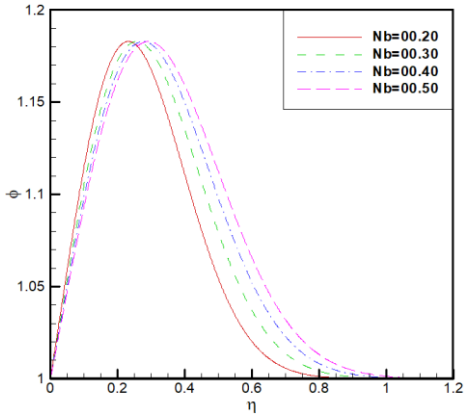

Fig. 15. Concentration profile for different values of Nb.

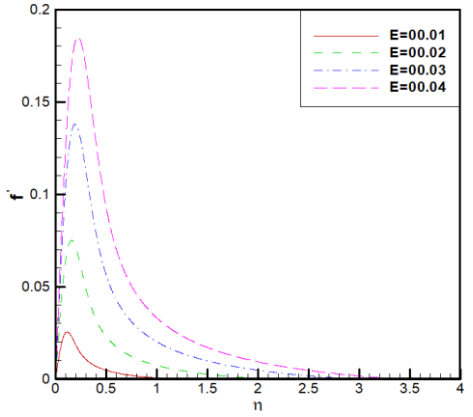

Fig. 16. Velocity profile for different values of E.

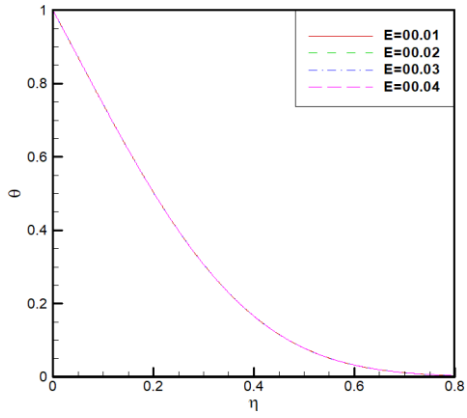

Fig. 17. Temperature profile for different values of E.

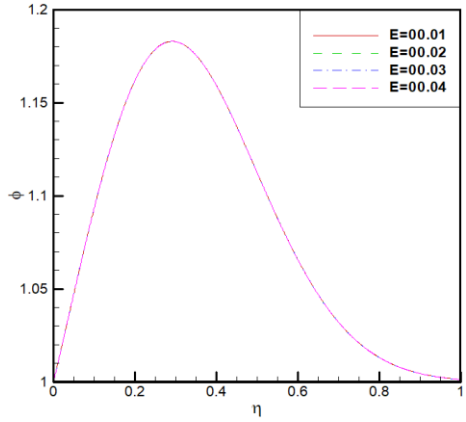

Fig. 18. Concentration profile for different values of E.

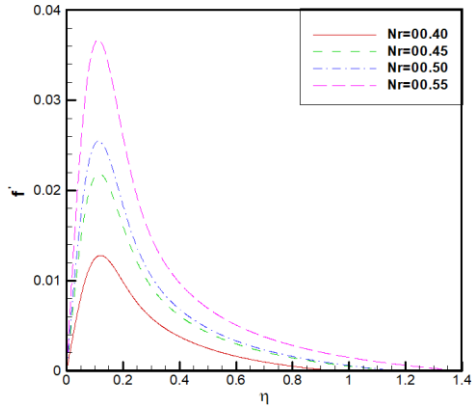

Fig. 19. Velocity profile for different values of Nr.

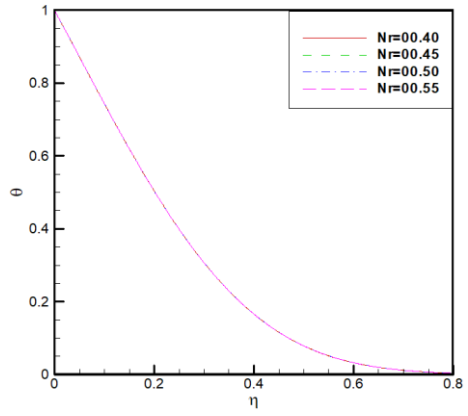

Fig. 20. Temperature profile for different values of Nr.

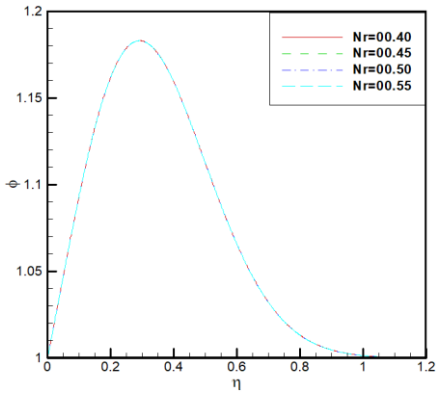

Fig. 21. Concentration profile for different values of Nr.

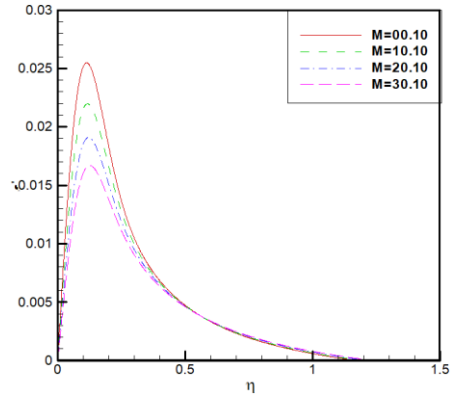

Fig. 22. Velocity profile for different values of M.

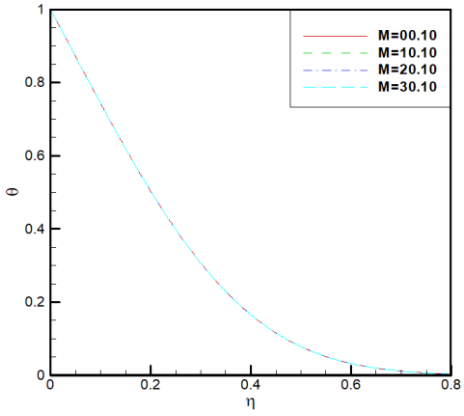

Fig. 23. Temperature profile for different values of M

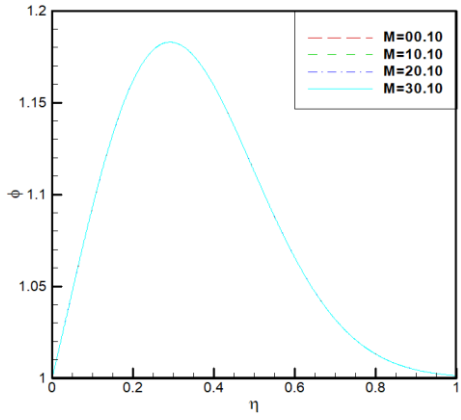

Fig. 24. Concentration profile for different values of M.

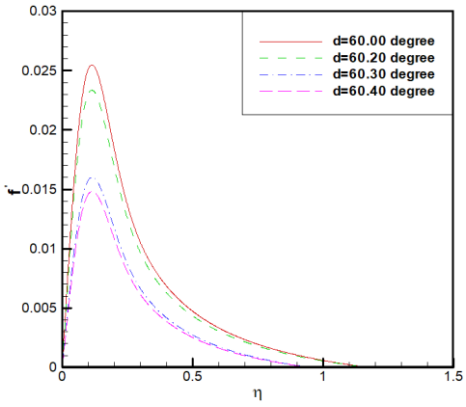

Fig. 25. Velocity profile for different values of d.

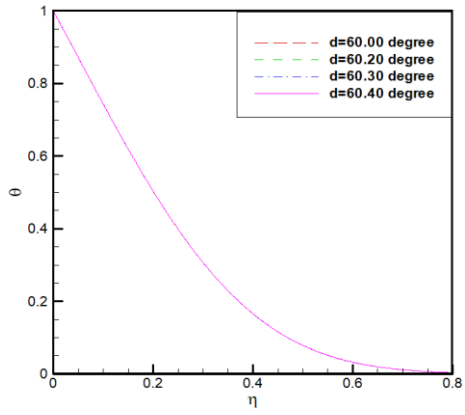

Fig. 26. Velocity profile for different values of d.

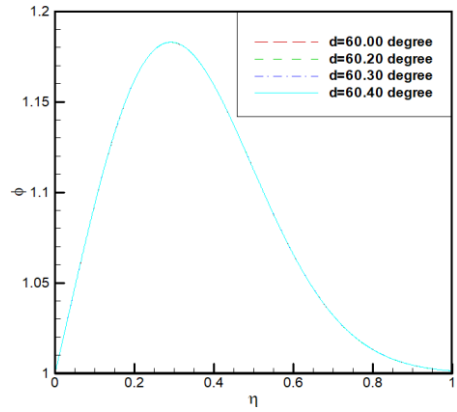

Fig. 27. Velocity profile for different values of d.

At last, numerical results are discussed in Tables 1-10 for the effect of several parameters on the Skin-friction coefficient, Nusselt number, and Sherwood number. Table 1 and Table 2 delineate that, Skin-friction coefficient, Nusselt number, and Sherwood number decrease with the increase of the magnetic M and thermal diffusivity parameter Bm.

Table 1. $f''(0)$, $\theta'(0)$, $\emptyset'(0)$ for several values of M.

M	$f''(0)$	$-\theta'(0)$	$\emptyset'(0)$
0.0	0.266488435	2.531689832	0.929650407
5.0	0.244718248	2.531689370	0.929649963
10.0	0.224986956	2.531688902	0.929649513
15.0	0.207060224	2.531688431	0.929649061

Table 2. $f''(0)$, $\theta'(0)$, $\emptyset'(0)$ for several values of Bm.

Bm	$f''(0)$	$-\theta'(0)$	$\emptyset'(0)$
0.10	0.266031360	2.531689823	0.929650398
0.14	0.220738952	2.114057097	0.691134212
0.18	0.182209924	1.849258998	0.550078139
0.22	0.148353839	1.663009380	0.456181391

Table 3. $f''(0)$, $\theta'(0)$, $\emptyset'(0)$ for several values of Nr.

Nr	$f''(0)$	$-\theta'(0)$	$\emptyset'(0)$
0.50	0.266031360	2.531689823	0.929650398
0.51	0.275779650	2.531689377	0.929649751
0.52	0.285527958	2.531688930	0.929649094
0.53	0.295276284	2.531688479	0.929648426

Table 4. $f''(0)$, $\theta'(0)$, $\emptyset'(0)$ for several values of E.

E	$f''(0)$	$-\theta'(0)$	$\emptyset'(0)$
0.01	0.266031360	2.531689823	0.929650398
0.02	0.690348449	2.531683368	0.929645489
0.03	1.104280109	2.531671157	0.929633656
0.04	1.305288981	2.531649821	0.929613008

Table 5. $f''(0)$, $\theta'(0)$, $\emptyset'(0)$ for different values of Nb.

Nb	$f''(0)$	$-\theta'(0)$	$\emptyset'(0)$
0.20	0.099776187	3.183129091	1.168692247
0.30	0.183871508	2.876531178	1.056266214
0.40	0.276322421	2.676949180	0.982999931
0.50	0.266031360	2.531689823	0.929650398

Table 6. $f''(0)$, $\theta'(0)$, $\emptyset'(0)$ for several values of P.

P	$f''(0)$	$-\theta'(0)$	$\emptyset'(0)$
0.30	0.305714003	2.531659128	1.859268112
0.40	0.285872732	2.531676328	1.394466753
0.50	0.273967924	2.531685012	1.115578607
0.60	0.266031360	2.531689823	0.929650398

Table 7. $f''(0)$, $\theta'(0)$, $\emptyset'(0)$ for different values of Nt.

Nt	$f''(0)$	$-\theta'(0)$	$\emptyset'(0)$
0.50	0.266031360	2.531689823	0.929650398
0.58	0.375637496	2.463419235	1.025241113
0.60	0.483590968	2.446061898	1.046625872
0.61	0.590892660	2.437506675	1.057081417

Table 8. $f''(0)$, $\theta'(0)$, $\emptyset'(0)$ for several values of Pr.

Pr	$f''(0)$	$-\theta'(0)$	$\emptyset'(0)$
1.0	0.266076166	2.531689823	0.929650398
3.0	0.266038826	2.531689823	0.929650398
5.0	0.266031360	2.531689823	0.929650398
7.0	0.266028160	2.531689823	0.929650398

Table 9. $f''(0)$, $\theta'(0)$, $\emptyset'(0)$ for several values of Db.

DB	$f''(0)$	$-\theta'(0)$	$\emptyset'(0)$
0.10	0.266031360	2.531689823	0.929650398
0.20	0.295658171	2.601408880	1.171644545
0.30	0.318400656	2.641942002	1.310210182
0.40	0.446227040	2.673229753	1.411489454

Table 10. $f''(0)$, $\theta'(0)$, $\emptyset'(0)$ for several values of d.

d	$f''(0)$	$-\theta'(0)$	$\emptyset'(0)$
60.00	0.266031360	2.531689823	0.929650398
60.05	0.261443641	2.531690480	0.929651033
60.10	0.256202447	2.531691217	0.919651744
60.20	0.243813625	2.531692900	0.929653369

It is noted in Tables 3-5 that, with the increases of the buoyancy-ratio (*Nr*), the viscosity of the nanofluid (*E*) and Brownian motion (*Nb*) parameters, both Nusselt number and Sherwood number decrease while Skin-friction co-efficient increase. Moreover, Table 6 depicts that with the increase of the unsteadiness parameter (*P*), both Skin-friction co-efficient and Sherwood number decrease while the Nusselt number increases. From Table 7, it is observed that the increases of the thermophoresis parameter (*Nt*), Skin-friction co-efficient, and Sherwood number increase while the Nusselt number decrease. It is also seen in Table 8 that, with the increases of the Prandtl number (*Pr*), both the Nusselt number and Sherwood number are fixed, but the Skin friction coefficient decreases. It is shown in Table 9 that, with the increases of the Brownian diffusion coefficient parameter (*Db*), Skin-friction coefficient, Nusselt number, and Sherwood number increase. In Table 10, it is clear that the Nusselt number and Sherwood number increase while the Skin-friction co-efficient decrease with the increased angle (*d*).

6. Conclusion

A similarity solution for the unsteady MHD boundary layer flow of a nanofluid for free convection of an inclined plate is reported. The governing boundary layer equations are solved numerically using the shooting method, namely the Nachtsheim-Swigert iteration technique using FORTRAN software. The effects of the non-dimensional governing parameters on the velocity, temperature concentration profiles, Nusselt, and Sherwood Numbers are discussed and presented through graphs and tabular form.

The particular conclusions drawn from this study can be summarized as follows:

(a) The Brownian diffusion coefficient reduces the temperature profiles. At the same time, velocity and concentration profiles are increased with increasing Brownian diffusion coefficient parameters.

(b) The fluid's velocity profiles decreased with the thermal diffusivity parameter increase. The increasing thermal diffusivity parameters Bm causes decreasing concentration profiles, but at a certain time, the concentration profile reverses and increases the temperature profile.

(c) An increase in the unsteadiness parameter (P) leads to a fall in the velocity and concentration profiles.

(d) As the viscosity of the nanofluid parameter increase, the velocity profile also increases.

(e) The velocity and temperature profiles increase with the Brownian motion parameter (Nb) and thermophoresis parameter (Nt) increase.

(f) The velocity profiles increase with the increase of the Buoyancy-ratio parameter.

(g) The Magnetic field parameters (M) and angle (d) reduce the velocity profiles.

(h) The Skin-friction coefficient, Nusselt number, and Sherwood number decrease with the magnetic (M) and thermal diffusivity parameter (Bm) increase.

(i) With the increases of the buoyancy-ratio (Nr), the viscosity of the nanofluid (E) and Brownian motion (Nb) parameters, both Nusselt number and Sherwood number decrease while the Skin-friction co-efficient increase.

Acknowledgments

The authors are grateful to the authority of the Chittagong University of Engineering and Technology (CUET) for providing technical support during this research work at Simulation Lab, Department of Mathematics, CUET, Chittagong, Bangladesh.

References

1. A. A. Math, Viscous Dissipation Chem. React. **10**, 952 (2015).
2. S. U. Choi and J. A. Eastman, Enhancing Thermal Conductivity of Fluids with Nanoparticles (No. ANL/MSD/CP-84938; CONF-951135-29), (Argonne National Lab., IL United States, 1995).
3. A. V. Kuznetsov and D. A. and Nield, Int. J. Thermal Sci. **49**, 243 (2010). https://doi.org/10.1016/j.ijthermalsci.2009.07.015

4. M. J. Uddin, W. A. Khan, and A. I. Ismail, PLoS One **7**, ID e49499 (2012). https://doi.org/10.1371/journal.pone.0049499
5. M. Mustafa, A. Mushtaq, T. Hayat, and B. Ahmad, PLoS One **9**, ID 103946 (2014). https://doi.org/10.1371/journal.pone.0103946
6. P. Rana and R. Bhargava, Communicat. Nonlinear Sci. Numer. Simul. **17**, 212 (2012). https://doi.org/10.1016/j.cnsns.2011.05.009
7. G. C. Shit, R. Haldar, and S. K. Ghosh, Int. J. Appl. Comput. Math. **2**, 593 (2016). https://doi.org/10.1007/s40819-015-0080-4
8. M. Goyal and R. Bhargava, Int. Scholarly Res. Notices **2013**, ID 931021 (2013). https://doi.org/10.1155/2013/931021
9. G. Wang, Z. Zhang, R. Wang, and Z. Zhu, Nanomaterials 10, 2386 (2020). https://doi.org/10.3390/nano10122386
10. S. K. Nandy, S. Sidui, and T. R. Mahapatra, Alexandria Eng. J. **53**, 929 (2014). https://doi.org/10.1016/j.aej.2014.09.001
11. S. M. Ibrahim and N. B. Reddy, Int. Scholarly Res. Notices (2013). https://doi.org/10.1155/2013/790604
12. M. Goyal and R. Bhargava, Appl. Nanosci. **4**, 761 (2014). https://doi.org/10.1007/s13204-013-0254-5
13. M. Goyal and R. Bhargava, Microfluidics Nanofluidics **17**, 591 (2014). https://doi.org/10.1007/s10404-013-1326-2
14. F. Ali, I. Khan, and S. S. Samiulhaq, PloS one **8,** ID e65223 (2013). https://doi.org/10.1371/journal.pone.0065223
15. K. L. Walker, G. M. Homsy, and F. T. Geyling, J. Colloid Interface Sci. **69**, 138 (1979). https://doi.org/10.1016/0021-9797(79)90088-2
16. M. A. A. Hamad, I. Pop, and A. M. Ismail, Non-linear Analysis: Real World Applicat. **12**, 1338 (2011). https://doi.org/10.1016/j.nonrwa.2010.09.014
17. A. J. Chamkha and A. M. Aly, Chem. Eng. Communi. **198**, 425 (2010). https://doi.org/10.1080/00986445.2010.520232
18. M. Y. Ali, M. J. Uddin, M. N. Uddin, and N. M. R. Zahed, J. Sci. Res. **8**, 287 (2016). https://doi.org/10.3329/jsr.v8i3.27347
19. K. Venkatasubbaiah and T. K. Sengupta, Int. J. Thermal Sci. **48**, 461 (2009). https://doi.org/10.1016/j.ijthermalsci.2008.03.019
20. C. H. Johnson and C. Ping, Int. J. Heat Mass Transfer **21**, 709 (1978). https://doi.org/10.1016/0017-9310(78)90032-7
21. M. Kumari, A. Slaouti, H. S. Takhar, S. Nakamura, and G. Nath, Acta Mechanica **116**, 75 (1996). https://doi.org/10.1007/BF01171421
22. A. Slaouti, H. S. Takhar, and G. Nath, Int. J. Heat Mass Transfer **41**, 3397 (1998). https://doi.org/10.1016/S0017-9310(98)00080-5
23. M. A. A. Hamad, and I. Pop, Heat Mass Transfer **47**, ID 1517 (2011). https://doi.org/10.1007/s00231-011-0816-6
24. M. Y. Ali, N. M. R. Zahed, M. N. Uddin, and M. J. Uddin, J. Sci. Res. **8**, 341 (2016). https://doi.org/10.3329/jsr.v8i3.27851
25. M. Y. Ali, M. N. Uddin, M. J. Uddin, and N. R. Zahed, Open J. Fluid Dyn. **5**, 391 (2015). https://doi.org/10.4236/ojfd.2015.54038
26. M. N. Uddin, M. Y. Ali, N. R. Zahed, and M. J. Uddin, Open J. Fluid Dyn. **6**, 279 (2016). https://doi.org/10.4236/ojfd.2016.64022